



Society of Petroleum Engineers

SPE-193906-MS

Flexible Discretizations of the Three-Component Three-Phase Flow Problem

Loic Cappanera and Beatrice Riviere, Rice University

Copyright 2019, Society of Petroleum Engineers

This paper was prepared for presentation at the SPE Reservoir Simulation Conference held in Galveston, Texas, USA, 10–11 April 2019.

This paper was selected for presentation by an SPE program committee following review of information contained in an abstract submitted by the author(s). Contents of the paper have not been reviewed by the Society of Petroleum Engineers and are subject to correction by the author(s). The material does not necessarily reflect any position of the Society of Petroleum Engineers, its officers, or members. Electronic reproduction, distribution, or storage of any part of this paper without the written consent of the Society of Petroleum Engineers is prohibited. Permission to reproduce in print is restricted to an abstract of not more than 300 words; illustrations may not be copied. The abstract must contain conspicuous acknowledgment of SPE copyright.

Abstract

A discontinuous Galerkin method of first order is proposed to solve the three-phase flow problem in three-dimensional heterogeneous reservoirs. The formulation is based on the compositional model and the primary unknowns are the total mass fraction of gas, the aqueous phase saturation and the liquid phase pressure. The algorithm is sequential and controls the nonlinearity with a subiteration scheme. Robustness of the method is shown on reservoirs with different heterogeneities: random permeability field, reservoir with barriers and layered reservoir. The algorithm easily handles phase appearance and disappearance, as well as mass transfer between the vapor and liquid phase.

Introduction

The study of three-phase flow in porous media is important as it is a popular model in petroleum engineering and in upstream industry. This work formulates a numerical model for three-component (oil, gas, water) and three-phase (liquid, vapor, aqueous) flow. Typically, the conventional black-oil model is used for modeling three-component three-phase flows where the hydrocarbons are grouped in pseudo-components. Black-oil models are common and are computationally cheaper than compositional models. However, conventional black-oil models do not easily handle phase appearance and disappearance (Forsyth 1984). A compositional-based formulation of the black-oil problem has been proposed to remediate this difficulty (Shank & Vestal 1989). Following this formulation, the choice of primary unknowns is the liquid phase pressure, the aqueous phase saturation, and the total mass fraction of gas. Our model assumes that mass transfer occurs between the liquid and vapor phase. Because the formulation is based on the compositional model, either flash or differential physical data can be used. The novelty of this work is the discretization of the equations based on locally mass conservative discontinuous Galerkin methods. The liquid phase pressure equation is solved by the incomplete interior penalty discontinuous Galerkin method, the aqueous phase saturation equation and the total mass fraction of gas equation are solved by the non-symmetric interior penalty discontinuous Galerkin method. The nonlinear system of equations is solved sequentially and a subiteration scheme is employed for higher accuracy. The general algorithm is described in the work by Cappanera and Riviere (2018), where it was applied to homogeneous reservoirs. The contribution of this work is to show the robustness of the numerical method for highly heterogeneous reservoirs.

Discontinuous Galerkin (DG) methods have gained popularity in modeling two-phase flows in porous media for over ten years, either by themselves or combined with other methods (see for instance [Klieber & Riviere 2006](#), [Hoteit & Firoozabadi 2008](#), [Natvig & Lie 2008](#), [Ern & Mozolevski & Schuh 2010](#), [Arbogast, Juntunen, Pool & Wheeler 2013](#), [Bastian 2014](#)). These methods are locally mass conservative like the popular finite volume methods. DG methods achieve higher accuracy and exhibit much less numerical diffusion. The application of DG methods to three-phase flows without or with mass transfer has been rare. Two-component two-phase flow with mass transfer, using liquid pressure and dissolved hydrogen density as primary unknowns, was approximated by a DG method of first order in one-dimensional reservoirs in the work of [Ern & Mozolevski \(2012\)](#). A DG method up to fourth order was proposed for the conventional black-oil model for saturated and undersaturated one-dimensional reservoirs in the work of [Rankin & Riviere \(2015\)](#). An iterative implicit pressure-explicit saturation method based on the local discontinuous Galerkin method was applied to the conventional black-oil model by [Wang, Zhang & Chen \(2015\)](#). In this work, we apply a sequential DG method of first order to three-dimensional heterogeneous reservoirs. The phase velocities are locally projected onto discrete subspaces of $H(\text{div})$, namely the Raviart-Thomas spaces ([Raviart & Thomas 1977](#), [Ern, Nicaise & Vohralik 2007](#)). For the numerical fluxes of the elliptic operators, we use the weighted averages proposed in [Ern, Stephansen & Zunino \(2008\)](#) and the weighted penalty values of [Bastian \(2014\)](#).

The outline of the paper is as follows. We first present the formulation of the problem and its discretization. The numerical results include several simulations in three-dimensional reservoirs with various types of heterogeneities. Conclusions follow.

Numerical Model

We first introduce the differential equations satisfied by the primary unknowns, and then describe the sequential algorithm.

Problem equations

We select for primary unknowns the liquid phase pressure, p_l , the aqueous phase saturation, S_a , and the total fraction of gas in the reservoir, z_g , defined by

$$z_g = x_{g,l} \frac{\rho_l S_l}{\rho_l S_l + \rho_v S_v + \rho_a S_a} + x_{g,v} \frac{\rho_v S_v}{\rho_l S_l + \rho_v S_v + \rho_a S_a}.$$

For each phase α , the phase saturation is denoted by S_α , the phase density by ρ_α and the mass fraction of the gas component in the liquid phase and in the vapor phase are denoted by $x_{g,l}$ and $x_{g,v}$ respectively.

The primary unknowns satisfy the system of coupled nonlinear partial differential equations:

$$\frac{\partial}{\partial t} (\phi \rho_t) - \nabla \cdot ((\rho \lambda)_t \nabla p_l) - \nabla \cdot (\rho_v \lambda_v \nabla p_{c,v}) + \nabla \cdot (\rho_a \lambda_a \nabla p_{c,a}) = (\rho q)_t, \quad (1)$$

$$\frac{\partial}{\partial t} (\phi \rho_a S_a) - \nabla \cdot (\rho_a \lambda_a \nabla p_a) = \rho_a q_a, \quad (2)$$

$$\frac{\partial}{\partial t} (\phi \rho_t z_g) - \nabla \cdot (F_g (\rho \lambda)_t \nabla p_l) - \nabla \cdot (x_{g,v} \rho_v \lambda_v \nabla p_{c,v}) = x_{g,l} \rho_l q_l + x_{g,v} \rho_v q_v, \quad (3)$$

where we have used the following shorthand notation

$$\rho_t = \rho_l S_l + \rho_a S_a + \rho_v S_v, \quad (\rho \lambda)_t = \rho_l \lambda_l + \rho_a \lambda_a + \rho_v \lambda_v, \quad (\rho q)_t = \rho_l q_l + \rho_a q_a + \rho_v q_v.$$

The phase mobilities are denoted by λ_α and the fractional flow is defined as

$$F_g = x_{g,l} F_{g,l} + x_{g,v} F_{g,v}, \quad F_{g,l} = \frac{\rho_l \lambda_l}{(\rho \lambda)_t}, \quad F_{g,v} = \frac{\rho_v \lambda_v}{(\rho \lambda)_t}.$$

Equations (1), (2) and (3) are completed by boundary conditions and initial conditions. In the rest of the paper, K denotes the absolute permeability. We end this section by recalling the definition of capillary pressures:

$$p_{c,v} = p_v - p_l = p_{c,v}(S_v), \quad p_{c,a} = p_l - p_a = p_{c,a}(S_a).$$

Full discretization

Equations (1), (2) and (3) are discretized in space by the interior penalty discontinuous Galerkin method (Riviere 2008). The reservoir is partitioned into hexaedra and each unknown is approximated by a discontinuous piecewise linear polynomial. The algorithm solves for each primary unknown sequentially at each time step, with a subiteration scheme loop. The incomplete interior penalty discontinuous Galerkin is used to solve the pressure equation whereas the non-symmetric interior penalty discontinuous Galerkin method is used for the saturation and mass fraction equations. Let τ denote the time step. The iterations are initialized with the unknowns at the previous time step. Let (p_l^n, S_a^n, z_g^n) denote the solutions at the previous time step and let (P^k, S^k, Z^k) denote the k -th iterate.

Step 0: initialization

$$(P^0, S^0, Z^0) = (p_l^n, S_a^n, z_g^n).$$

Step 1: pressure equation: solve for P^{k+1} satisfying

$$\frac{\phi(\rho_t^k - \rho_t^n)}{\tau} - \nabla \cdot ((\rho\lambda)_t^k \nabla P^{k+1}) - \nabla \cdot (\rho_v^k \lambda_v^k \nabla p_{c,v}^n) + \nabla \cdot (\rho_a^k \lambda_a^k \nabla p_{c,a}^n) = (\rho q)_t^{k+1}.$$

Using the iterate P^{k+1} , update the mass fractions $x_{g,l}^{k+1}, x_{g,v}^{k+1}, x_{o,l}^{k+1}, x_{o,v}^{k+1}$ and the phase densities $\rho_l^{k+1}, \rho_v^{k+1}$ and compute the projected velocity, denoted by \mathbf{u}_1^{k+1} , of the quantity $-K\nabla P^{k+1}$, and the projected velocity, denoted by \mathbf{u}_2^{k+1} , of the quantity $-(\rho_l^{k+1} \lambda_l^k + \rho_v^{k+1} \lambda_v^k + \rho_a \lambda_a^k) \nabla P^{k+1}$, into the Raviart-Thomas space of first order.

Step 2: saturation equation: solve for S^{k+1} satisfying

$$\begin{aligned} \frac{\phi \rho_a (S^{k+1} - S_a^n)}{\tau} + \nabla \cdot \left(\rho_a \lambda_a^k \left(\frac{\partial p_{c,a}}{\partial S_a} \right)^k \nabla S^{k+1} \right) \\ = \rho_a q_a^{n+1} - \nabla \cdot \left(\rho_a \lambda_a^k \left(\frac{\partial p_{c,a}}{\partial S_v} \right)^k \nabla S_v^k \right) + \nabla \cdot \left(\rho_a \frac{\kappa_{ra}^k}{\mu_a} \mathbf{u}_1^{k+1} \right) \end{aligned}$$

Using the iterate S^{k+1} , we update the relative permeability of the aqueous phase, κ_{ra}^{k+1} .

Step 3: mass fraction equation: solve for Z^{k+1} satisfying

$$\begin{aligned} \frac{\phi(\rho_t^{*,k+1} Z^{k+1} - \rho_t^{*,n} z_g^n)}{\tau} + \nabla \cdot \left((F_g^k + \left(\frac{\partial F_g}{\partial z_g} \right)^k (Z^{k+1} - Z^k)) \mathbf{u}_2^{k+1} \right) \\ - \nabla \cdot \left(x_{g,v}^{k+1} \rho_v^{k+1} \lambda_v^k \left(\frac{\partial p_{c,v}}{\partial S_v} \right)^k (A \nabla Z^{k+1} - B \nabla Z^k + E) \right) = x_{g,l}^{k+1} \rho_l^{k+1} q_l^{n+1} + x_{g,v}^{k+1} \rho_v^{k+1} q_v^{n+1}, \end{aligned}$$

where the variables A, B, E are defined below:

$$A = \frac{\rho_l^k \rho_v^k (x_{g,v}^k - x_{g,l}^k)(1 - S^{k+1}) + \rho_a^k \rho_v^k x_{g,v}^k S^{k+1}}{\left((x_{g,v}^k - Z^k) \rho_v^k + (Z^k - x_{g,l}^k) \rho_l^k \right)^2}, B = \frac{\rho_a^k \rho_l^k x_{g,v}^k S^{k+1}}{\left((x_{g,v}^k - Z^k) \rho_v^k + (Z^k - x_{g,l}^k) \rho_l^k \right)^2},$$

$$E = \left(\frac{\partial S_v}{\partial x_{g,l}} \right)^k \nabla x_{g,l}^{k+1} + \left(\frac{\partial S_v}{\partial x_{g,v}} \right)^k \nabla x_{g,v}^{k+1} + \left(\frac{\partial S_v}{\partial \rho_a} \right)^k \nabla \rho_a^{k+1} + \left(\frac{\partial S_v}{\partial \rho_l} \right)^k \nabla \rho_l^{k+1} + \left(\frac{\partial S_v}{\partial \rho_v} \right)^k \nabla \rho_v^{k+1}.$$

Next, update the relative permeabilities and saturations of the liquid and vapor phases.

Step 4: set $k \leftarrow k + 1$ and repeat steps 1 to 3 until convergence of the iterates.

Numerical Results

The proposed method is applied to reservoirs with various permeability fields. The first three examples study the impact of random permeability fields, of layered permeability fields and of barriers in the reservoirs on three-phase flows without mass transfer between the phases. The fourth example allows for mass transfer to occur between the liquid and vapor phase as the pressure varies in the reservoir. All the units are SI, unless explicitly stated. The computations were performed with the fully parallel framework Dune developed by Bastian et al (2008a, 2008b).

Random permeability

We consider a three-dimensional domain with dimensions $[0,1000] \times [0,100] \times [0,100]$. The reservoir is initially filled with a mixture of liquid and vapor phases by setting

$$(S_l, S_v, S_a)_{t=0} = (0.8, 0.2, 0).$$

The initial pressure is defined as follows:

$$p_l(x, y, z, t = 0) = 2 \times 10^8 - 10^5 x.$$

Dirichlet boundary conditions that match the liquid pressure initial condition are applied on the faces ($x = 0$) and ($x = 1000$). The following boundary conditions are enforced on the aqueous and vapor saturations:

$$S_a(x = 0, y, z, t) = \frac{10^{-15} t^3}{10(1 + 10^{-15} t^3)}, \quad S_v(x = 0, y, z, t) = 0.4 + \frac{10^{-15} t^3}{2(1 + 10^{-15} t^3)}.$$

Homogeneous Neumann conditions are applied on the remaining boundaries. The physical properties of the fluid and medium are:

$$\mu_l = \mu_a = 10^{-3}, \quad \mu_v = 10^{-4}, \quad \rho_l = 800, \quad \rho_v = 400, \quad \rho_a = 1000, \quad \phi = 0.2.$$

Capillary pressures and relative permeabilities are chosen as:

$$\kappa_{rl} = S_l^2, \quad \kappa_{rv} = S_v^2, \quad \kappa_{ra} = S_a^2,$$

$$p_{c,v} = \begin{cases} -A_{pc} S_v^{-0.5} & \text{if } S_v > 0.05 \\ 0.05^{-0.5} A_{pc} (-1.5 + 10 S_v) & \text{otherwise} \end{cases}, \quad p_{c,a} = \begin{cases} A_{pc} S_a^{-0.5} & \text{if } S_a > 0.05 \\ 0.05^{-0.5} A_{pc} (1.5 - 10 S_a) & \text{otherwise} \end{cases}.$$

The constant A_{pc} is specified later and will take different values. In this section, there is no mass transfer and we set:

$$x_{g,l} = x_{o,v} = 0.$$

The absolute permeability of the reservoir is equal to $(3.12 \times 10^{-15})K_{rand}$, where K_{rand} is a piecewise constant function that takes random values in the interval [100,2100]. Figure 1 displays the permeability field in a three-dimensional view and in the slice ($y = 50$).

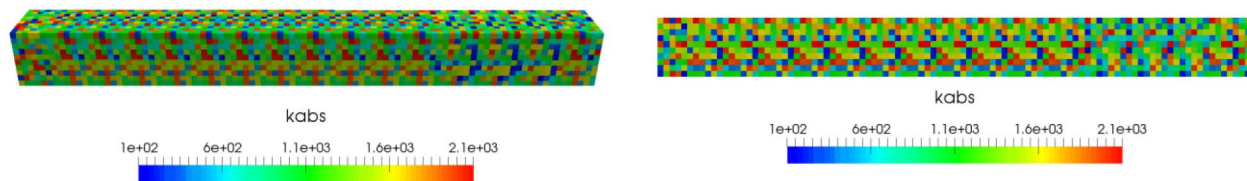


Figure 1—Three-dimensional view (left) and slice view (right) of the random multiplicative factor. Permeability field is obtained by multiplying by 3.12×10^{-15} .

Snapshots of the liquid saturation are shown in Figure 2 at two different times. The entry pressure is $A_{pc} = 10^7$.

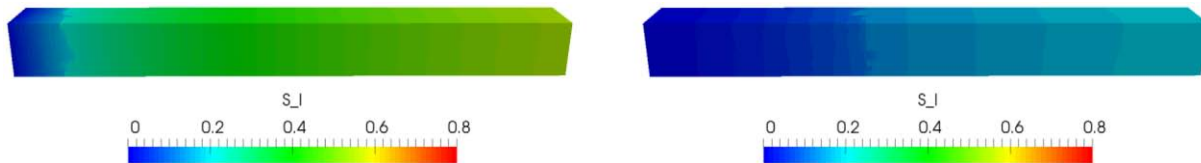


Figure 2—Liquid phase saturation at $t=4.63$ days (left) and $t=23.15$ days (right) with high capillary pressure.

We repeat the experiment with a lower amount of capillary pressure by setting $A_{pc} = 10^5$. Figure 3 shows the liquid phase saturation at two distinct times. We observe that fingers appear as the saturation front is less diffusive than in the high capillary case.

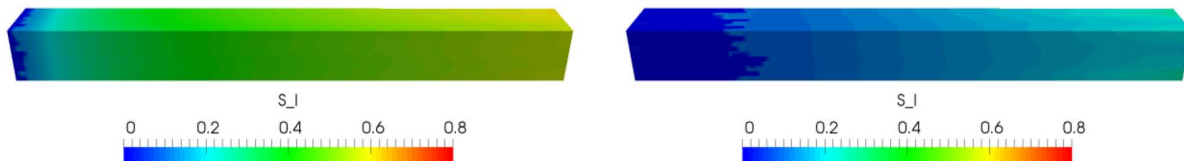


Figure 3—Liquid phase saturation at $t=4.63$ days (left) and $t=23.15$ days (right), with low capillary pressure.

Finally we show in Figure 4 the time evolution of the saturation of each phase at the location (200,50,50) in the reservoir for both high and low values of A_{pc} . We observe that for both cases, the saturation of aqueous and vapor phases increase while the liquid phase saturation decreases and eventually the liquid phase disappears. When capillary pressure is reduced, the aqueous phase saturation front reaches the location later.

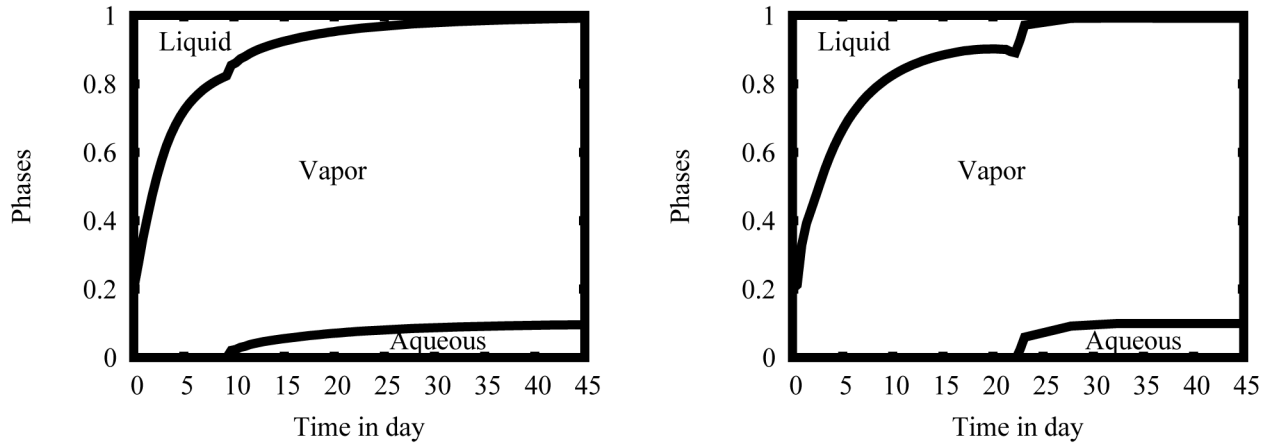


Figure 4—Time evolution of the saturation phases at the point (200,50,50): with $A_{pc} = 10^7$ (left) and $A_{pc} = 10^5$ (right).

Layered medium

In this experiment, we inject both vapor and aqueous phases in the reservoir. We study the effect of viscosities by first considering the case of equal viscosities and second the case where the vapor viscosity is ten times smaller than the aqueous viscosity. The setup is similar than in the previous example, except for the following data. Initially the reservoir is filled with both liquid and vapor phases:

$$(S_l, S_v, S_a)_{t=0} = (0.9, 0.1, 0).$$

Both vapor and aqueous phases are injected at the inflow face of the reservoir, via Dirichlet boundary conditions:

$$S_v(x=0, y, z, t) = 0.1 + \frac{8 \times 10^{-15} t^3}{10(1 + 10^{-15} t^3)}, \quad S_a(x=0, y, z, t) = \frac{10^{-15} t^3}{1 + 10^{-15} t^3}.$$

The absolute permeability increases with the vertical direction:

$$K = \begin{cases} 3.12 \times 10^{-15} K_{rand,1} & \text{if } 70 \leq z, \\ 3.12 \times 10^{-15} K_{rand,2} & \text{if } 30 \leq z \leq 70, \\ 3.12 \times 10^{-15} K_{rand,3} & \text{otherwise.} \end{cases}$$

where $K_{rand,1}$, $K_{rand,2}$, $K_{rand,3}$ are random functions such that $K_{rand,1} \in [100, 2100]$, $K_{rand,2} \in [10, 210]$ and $K_{rand,3} \in [1, 21]$. This means that the top layer in the reservoir is more permeable on average than the middle and bottom layers. Figure 5 displays the permeability field in a three-dimensional view and in the slice ($y=50$).

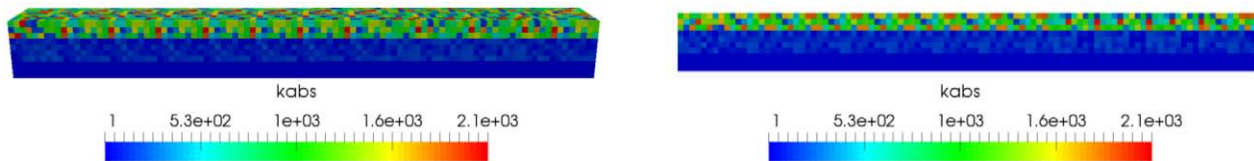
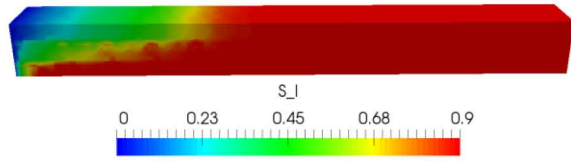
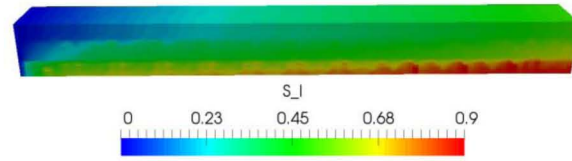
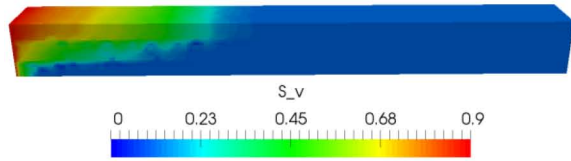
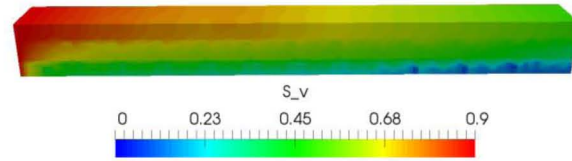
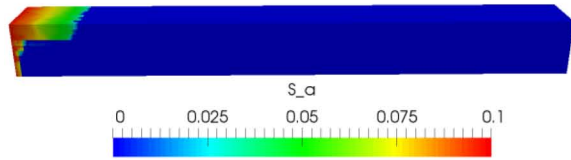
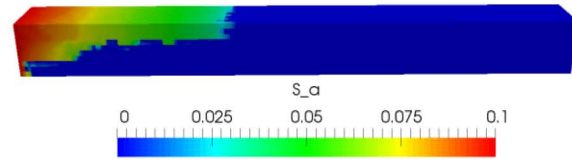


Figure 5—Three-dimensional view (left) and slice view (right) of the random functions. Permeability field is obtained by multiplying by 3.12×10^{-15} .

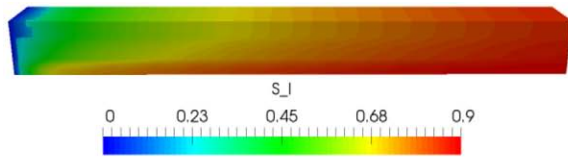
First we assume that $\mu_v = 10^{-3}$. Figure 6 shows the snapshots for each phase saturation at two distinct times. The phases first move through the regions with larger average permeability.

(a) *Liquid phase saturation $t = 4.63$ days*(b) *Liquid phase saturation $t = 23.15$ days*(c) *Vapor phase saturation $t = 4.63$ days*(d) *Vapor phase saturation $t = 23.15$ days*(e) *Aqueous phase saturation $t = 4.63$ days*(f) *Aqueous phase saturation $t = 23.15$ days***Figure 6—Phase saturations at two distinct times in the stratified reservoir at early and late times.**

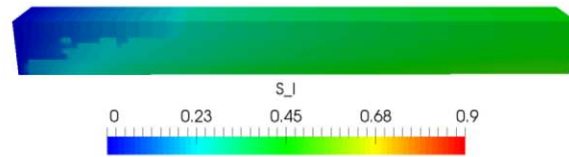
We now repeat the experiments with

$$\mu_v = 10^{-4}.$$

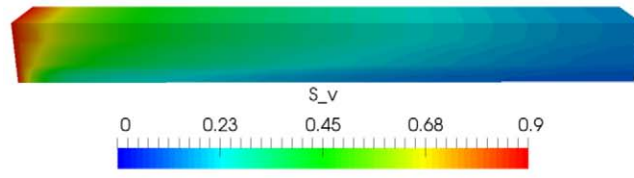
Figure 7 shows the phase distributions at different times. This set-up is more favorable to the flow of the vapor phase as it competes with the aqueous phase.



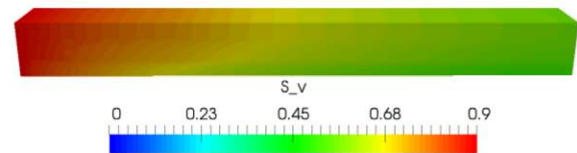
(a) *Liquid phase saturation $t = 4.63$ days*



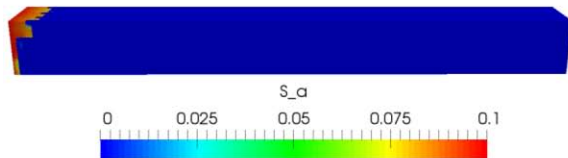
(b) *Liquid phase saturation $t = 23.15$ days*



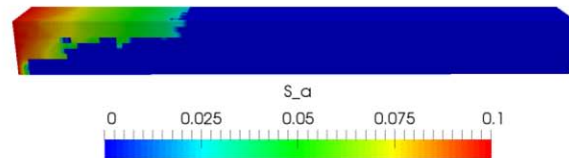
(c) *Vapor phase saturation $t = 4.63$ days*



(d) *Vapor phase saturation $t = 23.15$ days*



(e) *Aqueous phase saturation $t = 4.63$ days*



(f) *Aqueous phase saturation $t = 23.15$ days*

Figure 7—Phase saturations in the stratified reservoir at early and late times.

To better visualize the effect of the heterogeneities and the viscosities on the phase distributions, we show in Figure 8 the time evolution of the phases at two different points in the reservoir. One location is chosen in the middle layer, and the other location is in the top layer.

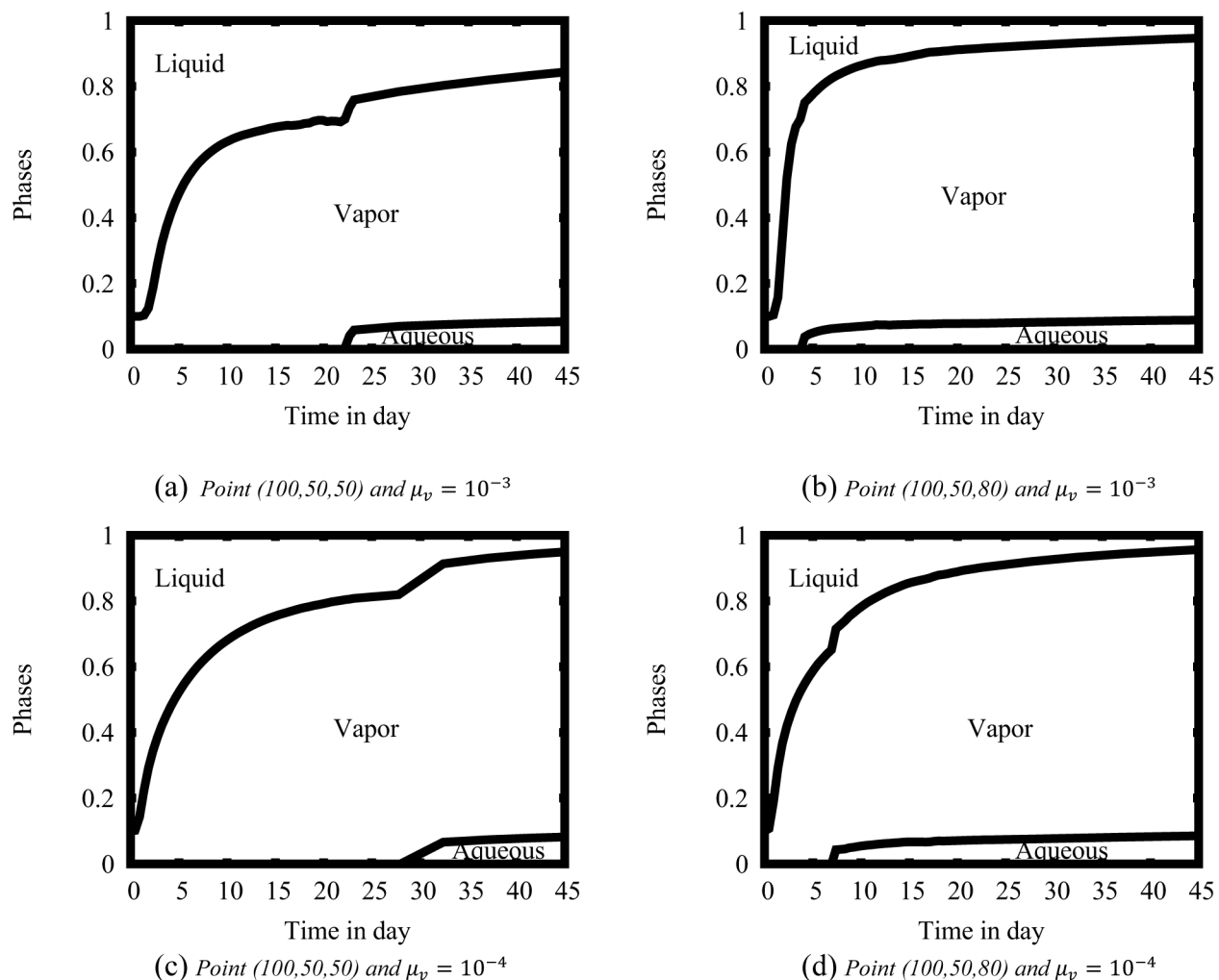


Figure 8—Time evolution of phase saturations in middle layer (left) and top layer (right) for different vapor viscosities.

Reservoir with barriers

In this experiment, the porous medium has the same dimensions as for the layered medium, and is characterized by a heterogeneous permeability field and several barriers in a section of the reservoir. The absolute permeability of the reservoir is equal to $(3.12 \times 10^{-15})K_{rand}$, where K_{rand} is a piecewise constant function that takes random values in the interval [100,2100]. Barriers are created in the section $[200,400] \times [0,100] \times [0,100]$ by reducing the range of K_{rand} to the interval [1,21]. Figure 9 shows a 3D representation of the permeability and a 2D view corresponding to the slice ($x = 300$).

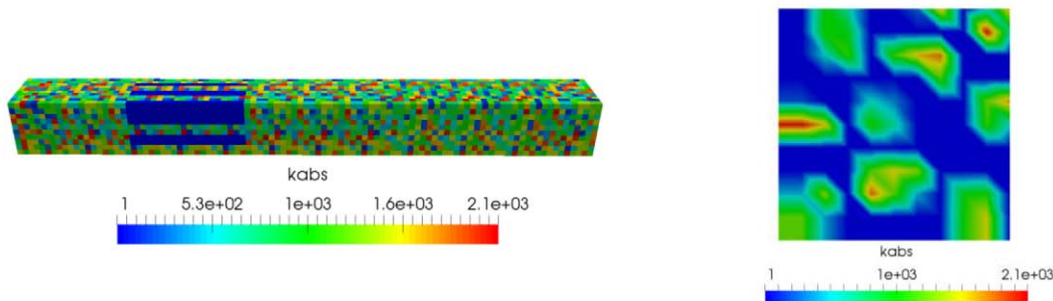


Figure 9—Distribution of the random permeability K_{rand} : 3D view (left) and 2D view for slice ($x = 300$) (right). The absolute permeability is multiplied by 3.12×10^{-15} .

Except for the permeability, the input data and setup are similar to those for the layered reservoir with vapor viscosity equal to 10^{-4} . The vapor saturation is shown in Figure 10 using the threshold $S_v \geq 0.25$, for better visualization of the front. The entry pressure is chosen as $A_{pc} = 10^7$. We observe that the barriers have little impact on the saturation propagation. We repeat the simulations with lower values $A_{pc} = 10^6$ and $A_{pc} = 10^5$. The threshold vapor phase saturation is shown at two distinct times in Figure 11 and Figure 12. We observe that fingers occur as the vapor phase does not easily flow in the barriers and even avoids them altogether for the smaller value of capillary pressure.

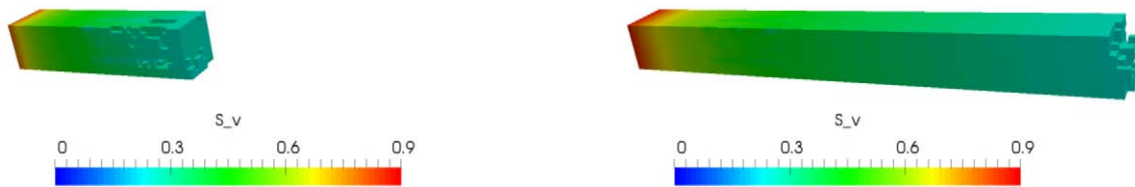


Figure 10—Threshold of the vapor phase saturation at time $t = 2.31$ days (left) and $t = 3.7$ days (right). Minimum value is 0.25 and maximum value is 0.9. Case: $A_{pc} = 10^7$.

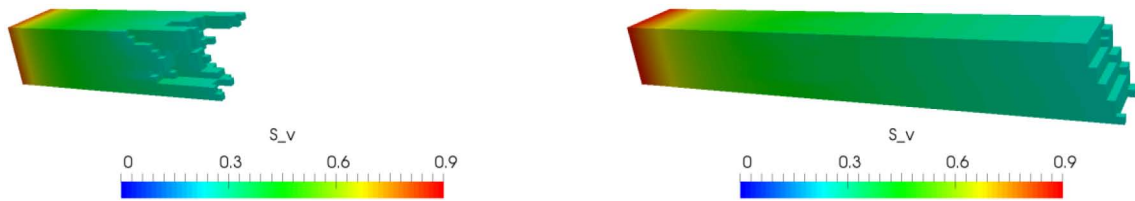


Figure 11—Threshold of the vapor phase saturation at time $t = 2.31$ days (left) and $t = 3.7$ days (right). Minimum value is 0.25 and maximum value is 0.9. Case: $A_{pc} = 10^6$.

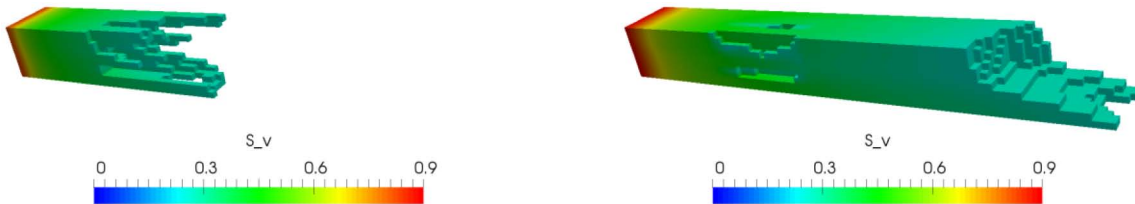


Figure 12—Threshold of the vapor phase saturation at time $t = 2.31$ days (left) and $t = 3.7$ days (right). Minimum value is 0.25 and maximum value is 0.9. Case: $A_{pc} = 10^5$.

We next show the aqueous phase saturation at different times. Because of smaller viscosity and smaller relative permeability, the aqueous phase saturation propagates slower than the vapor phase. The threshold values are shown for larger times (about ten times larger). Figure 13 shows the aqueous saturation with a threshold $0.01 \leq S_a \leq 0.1$ for the value $A_{pc} = 10^7$. Figure 14 and Figure 15 show the aqueous saturation at the same times with smaller values $A_{pc} = 10^6$ and $A_{pc} = 10^5$. We observe that fingers occur when A_{pc} decreases and the front moves more slowly.



Figure 13—Threshold of the aqueous phase saturation at time $t = 23$ days (left) and $t = 37$ days (right). Minimum value is 0.01 and maximum value is 0.1. Case: $A_{pc} = 10^7$.



Figure 14—Threshold of the aqueous phase saturation at time $t = 23$ days (left) and $t = 37$ days (right). Minimum value is 0.01 and maximum value is 0.1. Case: $A_{pc} = 10^6$.



Figure 15—Threshold of the aqueous phase saturation at time $t = 23$ days (left) and $t = 37$ days (right). Minimum value is 0.01 and maximum value is 0.1. Case: $A_{pc} = 10^5$.

Mass transfer

The following example is a three-phase flow simulation with mass transfer between the vapor and liquid phase for a heterogeneous medium. The gas component is in liquid phase for high pressure and as the pressure decreases, moves to the vapor phase. The water and oil components remain entirely in the aqueous and liquid phase respectively. Figure 16 shows the mass fraction $x_{g,l}$ and the density of the liquid phase ρ_l , as a function of liquid phase pressure. The gas component is in the vapor phase if the pressure is below 2×10^8 and forms 10% of the mass of liquid if the pressure is above 3×10^8 .

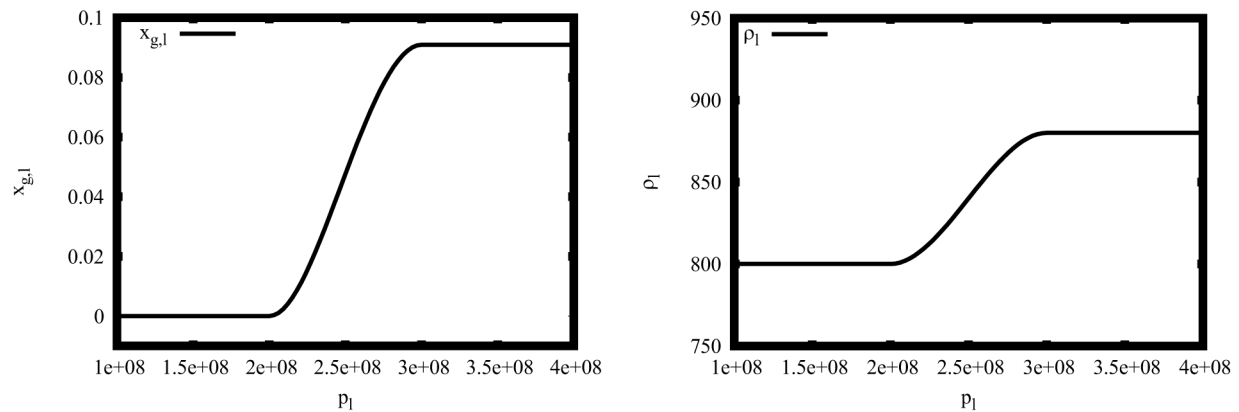


Figure 16—Mass fraction of gas in liquid phase (left) and liquid phase density (right) as functions of liquid phase pressure.

The reservoir is the domain $[0,1000] \times [0,100] \times [0,100]$. It is initially filled with liquid phase only with a composition of about 90% of oil and 10% of gas. The other characteristics are

$$\mu_l = \mu_a = 10^{-3}, \quad \mu_v = 10^{-4}, \quad \rho_v = 800, \quad \rho_a = 1000, \quad \phi = 0.2.$$

Relative permeabilities and capillary pressures are the same as in the previous experiments with $A_{pc} = 10^7$. Initial pressure and boundary conditions are defined below:

$$p_l(x, y, z, t = 0) = 4 \times 10^8 - 10^5 x,$$

$$S_a(x = 0, y, z, t) = \frac{10^{-15} t^3}{10(1 + 10^{-15} t^3)},$$

$$p_l(x = 0 \text{ or } 10^3, y, z, t) = 4 \times 10^8 - 10^5 x - \frac{2 \times 10^{-7} t^3}{1 + 10^{-15} t^3},$$

$$S_l(x = 0, y, z, t) = \begin{cases} 1 - S_a|_{x=0} & \text{if } p_l|_{x=0} \geq 3 \times 10^8, \\ 1 - S_a|_{x=0} - (2.7 - 9p_l|_{x=0} \times 10^{-9}) & \text{if } 2 \times 10^8 \leq p_l|_{x=0} < 3 \times 10^8, \\ 0 & \text{otherwise.} \end{cases}$$

From the boundary condition on the pressure, we see that the magnitude of the pressure decreases with time such that the injected gas is in vapor phase after a few days. We recall that the liquid phase saturation is not a primary unknown and the definition of the total mass fraction of gas is used with the above conditions to obtain a Dirichlet boundary condition for z_g . Homogeneous Neumann boundary conditions are applied to p_l , S_a and z_g elsewhere. Finally the permeability of the medium is $K = (6.24 \times 10^{-13})K_{rand}$, where K_{rand} is a piecewise constant function that takes random values in. Figure 17 displays the permeability field in a three-dimensional view and in a slice.

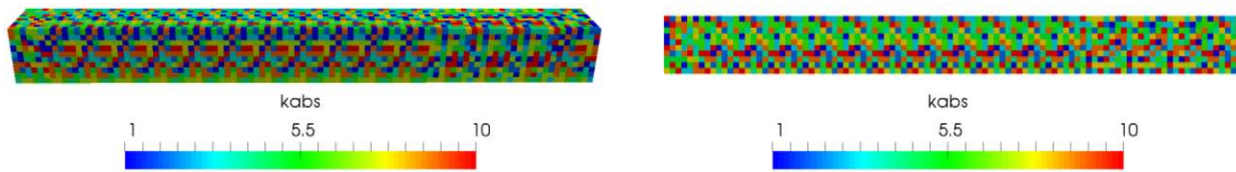


Figure 17—Random permeability field: 3D view (left) and 2D view in slice $y = 50$ (right). Absolute permeability is multiplied by 6.24×10^{-13} .

We show in Figure 18 the mass fraction $x_{g,l}$ along the line obtained by the intersection of the two planes ($y = 50$) and ($z = 50$), and at two different times. As time increases, the fraction of gas in the liquid phase tends to zero.

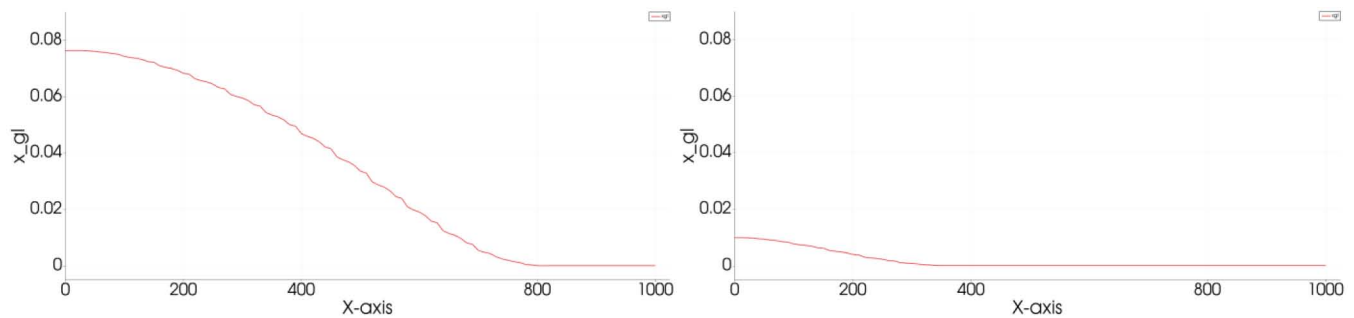


Figure 18—Profile of the mass fraction of gas in the liquid phase at $t=3.17$ days (left) and $t=4.86$ days (right).

The next figure shows the profile of each phase pressure along the same line (see Figure 19). The liquid pressure is shown in blue, the vapor pressure in green and the aqueous pressure in red. We observe that the liquid pressure is below 2×10^8 around $x = 800$ at $t = 3.17$ days and around $x = 300$ at $t = 4.86$ days, which are consistent results with the profile of the mass fraction of gas in the liquid phase in Figure 18.

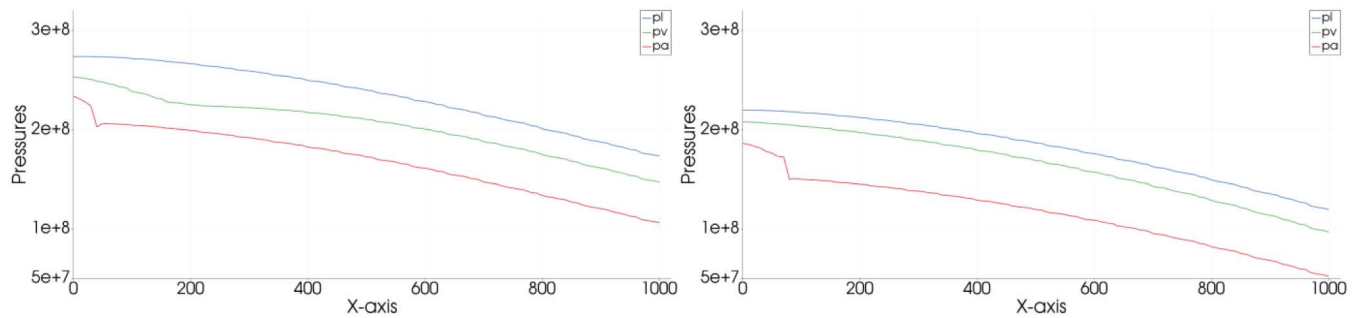


Figure 19—Profile of the liquid, aqueous and vapor phase pressure at t=3.17 days (left) and t=4.86 days (right).

The evolution of the phase saturations is shown at two different locations in the reservoir (see Figure 20). As time increases, the liquid phase saturation disappears.

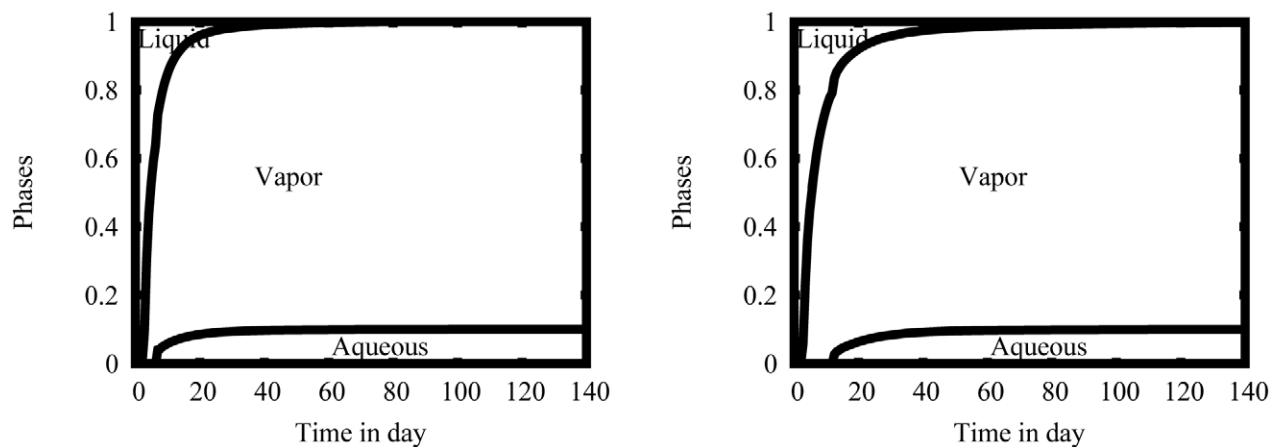


Figure 20—Time evolution of phase saturations at the location (100,50,50) (left) and at (200,50,50) (right).

Conclusions

This paper applies an algorithm to solve the three-phase flow without and with mass transfer in highly heterogeneous reservoirs. The primary unknowns are the liquid phase pressure, the aqueous phase saturation and the total mass fraction of gas. They are approximated by discontinuous polynomials of degree one. The algorithm solves for each unknown sequentially with a subiteration scheme to handle the nonlinearity. The pressure equation is solved with the incomplete interior penalty Galerkin whereas the saturation and mass fraction equations are solved with the non-symmetric interior penalty Galerkin method. No slope limiters are used. The paper shows the method is robust and can handle various types of heterogeneities in the permeability field, as well as phase appearance and disappearance and mass transfer between phases. Future work includes additional validation of the method and its extension to higher order.

Nomenclature

Notation	Physical quantity
ϕ	Porosity
S_α	Phase saturation
z_g	Total fraction of gas
p_α	Phase pressure
$p_{c,\alpha}$	Capillary pressure
$x_{i,\beta}$	Mass fraction of component i in phase α .
ρ_α	Phase density

λ_α	Phase mobility
μ_α	Phase viscosity
k_{ra}	Phase relative permeability
K	Absolute permeability

Bibliography

- Arbogast, T. & Juntunen, M. & Pool, J. & Wheeler, M.F. (2013). A discontinuous Galerkin method for two-phase flow in a porous medium enforcing H(div) velocity and continuous capillary pressure. *Computational Geosciences*, **17**(6), 1055–1078
- Bastian, P. & Blatt, M. & Dedner, A. & Engwer, C. & Klotforn, R. & Kornhuber, R. & Ohlberger, M. & Sander, O. (2008a). A generic grid interface for parallel and adaptive scientific computing. Part I: abstract framework. *Computing*, **82**, 121–138.
- Bastian, P. & Blatt, M. & Dedner, A. & Engwer, C. & Klotforn, R. & Kornhuber, R. & Ohlberger, M. & Sander, O. (2008b). A generic grid interface for parallel and adaptive scientific computing. Part II: implementation and tests in Dune. *Computing*, **82**, 121–138.
- Bastian, P. (2014). A fully-coupled discontinuous Galerkin method for two-phase flow in porous media with discontinuous capillary pressure. *Computational Geosciences*, **18**(5), 779–796
- Cappanera, L. & Riviere, B. (2018). Discontinuous Galerkin method for solving the black-oil problem in porous media. *Numerical Methods for Partial Differential Equations*. In press
- Ern, A. & Mozolevski, I., & Schuh, L. (2010). Discontinuous Galerkin approximation of two-phase flows in heterogeneous porous media with discontinuous capillary pressures. *Computer Methods in Applied Mechanics and Engineering*, **199**, 1491–1501
- Ern, A. & Mozolevski, I. (2012). Discontinuous Galerkin method for two-component liquid-gas porous media flows. *Computational Geosciences*, **16**, 677–690
- Ern, A. & Nicaise, S. & Vohralik, M. (2007). An accurate H(div) flux reconstruction for discontinuous Galerkin approximations of elliptic problems. *Comptes Rendus Mathématique*, **345**(12), 709–712
- Ern, A. & Stephansen, A.F. & Zunino, P. (2008). A discontinuous Galerkin method with weighted averages for advection-diffusion equations with locally small and anisotropic diffusivity. *IMA Journal of Numerical Analysis*, **29**(2), 235–256
- Forsyth, P. (1984). Gas phase appearance and disappearance in fully implicit black oil simulation. *SPE Journal*, SPE-11757-PA.
- Hoteit, H. & Firoozabadi, A. (2008). Numerical modeling of two-phase flow in heterogeneous permeable media with different capillary pressures. *Advances in Water Resources*, **31**(1) 56–73
- Klieber, W., & Riviere, B. (2006). Adaptive simulations of two-phase flow by discontinuous Galerkin methods. *Computer Methods in Applied Mechanics and Engineering*, **196**, 404–419
- Natvig, J. & Lie, K. (2008). Fast computational of multiphase flow in porous media by implicit discontinuous Galerkin schemes with optimal ordering of elements. *Journal of Computational Physics*, **227**, 10108–10124
- Rankin, R. & Riviere, B. (2015). A high order method for solving the black-oil problem in porous media. *Advances in Water Resource*, **78**, 126–144
- Raviart, P. & Thomas, J. (1977). A mixed finite element method for second order elliptic problems. *Mathematical Aspects of the Finite Element Method, Lecture Notes in Mathematics*, **606**, 292–315
- Riviere, B. (2008). *Discontinuous Galerkin Methods for Solving Elliptic and Parabolic Equations*. Philadelphia, PA, USA: Society for Industrial and Applied Mathematics.
- Shank, G., & Vestal, C. (1989). Practical techniques in two-pseudocomponent black-oil simulation. *SPE Reservoir Engineering*, **4**(2), 244–252
- Wang, K. & Zhang, L. & Chen, Z. (2015). Development of discontinuous Galerkin methods and a parallel simulator for reservoir simulation. *SPE*, SPE-176168-MS